Supporting Information

β-$Ni(OH)_2$ nanosheet: an effective sensing platform for constructing nucleic acid-based optical sensor

Hui Zhou,[a,b] Jun Bing Peng,[b] Xinlan Qiu,[a] Yan Sha Gao,[a] Limin Lu,*[a] Wenmin Wang [a]

a. College of Science, Jiangxi Agricultural University, Nanchang 330045, PR China.
b. College of Chemistry and Chemical Engineering, Gannan Normal University, Ganzhou 341000, China.

1. Experimental Section

Table S1. Sequences of miRNAs and DNA probes used in this work

Name	Sequence (5'-3')
5-F	FAM- CCA TC
9-F	FAM- CCA TCT TTA
13-F	FAM- CCA TCT TTA CCA G
17-F	FAM- CCA TCT TTA CCA GAC AG
22-F	FAM- CCA TCT TTA CCA GAC AGT GTT A
22-C	Cy3 - CCA TCT TTA CCA GAC AGT GTT A
P-141	FAM - CCA TCT TTA CCA GAC AGT GTT A -FAM
MB	FAM-**CCTCCAC**CCATCTTTACCAGACAGTGTTA**GTGGAGG**-BHQ1
miRNA-141	U AAC ACU GUC UGG UAA AGA UGG
miRNA-429	U AAU ACU GUC UGG UAA AAC CGU
miRNA-200b	U AAU ACU GCC UGG UAA UGA UGA
SmiRNA-141	U AAC ACU GUC UAG UAA AGA UGG
miRNA-21	U AGC UUA UCA GAC UGA UGU UGA
P-21	TAMRA - TCA ACA TCA GTC TGA TAA GCT A - TAMRA
DNA-141	T AAC ACT GTC TGG TAA AGA TGG

SmiRNA-141 is a single-base mismatched RNA, and the mismatched position is marked in red. The underlined sequence of MB is designed to recognize miRNA-141 and form MB/miRNA duplex. DNA-141 is a ssDNA with same sequences as miRNA-141.

2. Supplementary results

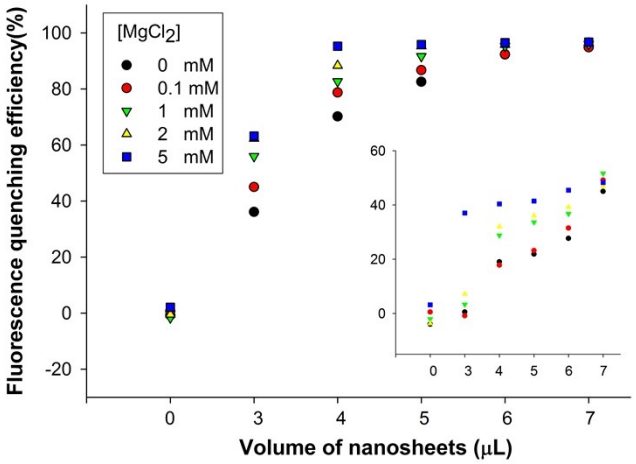

Fig. S1 Quenching efficiency as a function of β-$Ni(OH)_2$ nanosheets with ssDNA (inset is dsDNA) in the presence of varying concentrations of $MgCl_2$. The concentrations for β-$Ni(OH)_2$ nanosheets and DNA (ssDNA: 22-F; dsDNA: 22-F/DNA-141) were 480 μg/mL and 50 nM, respectively. The buffer used in this experiment is 25 mM Tris-HCl (pH=8.0) containing 100 mM KCl.

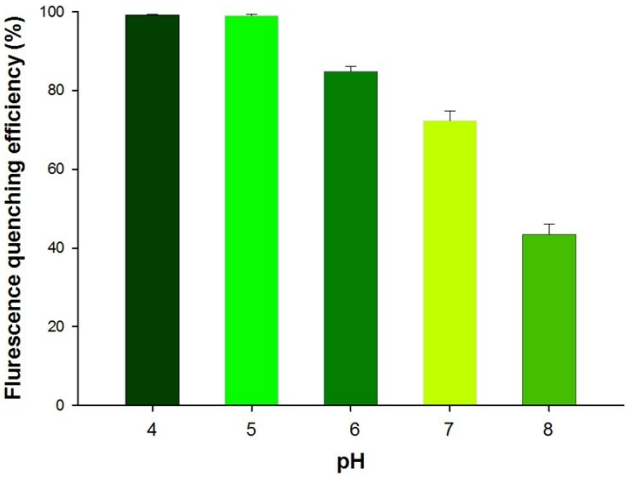

Fig. S2 Effect of pH on the quenching efficiency between β-$Ni(OH)_2$ nanosheets and ssDNA.. Each sample was prepared in 25 mM buffer containing 100 mM KCl, 1 mM $MgCl_2$, 84 μg/mL β-$Ni(OH)_2$ nanosheets and 600 nM 22-F ssDNA.

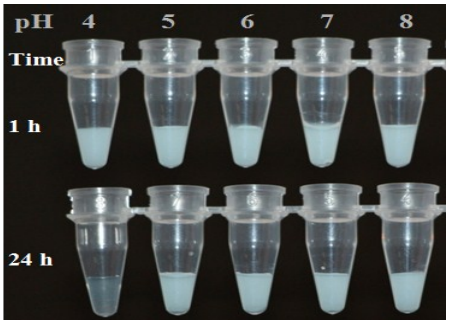

Fig. S3 Effect of pH on the degradation of β-$Ni(OH)_2$ nanosheets. Each sample contains 2.4 mg/mL β-$Ni(OH)_2$ nanosheets.

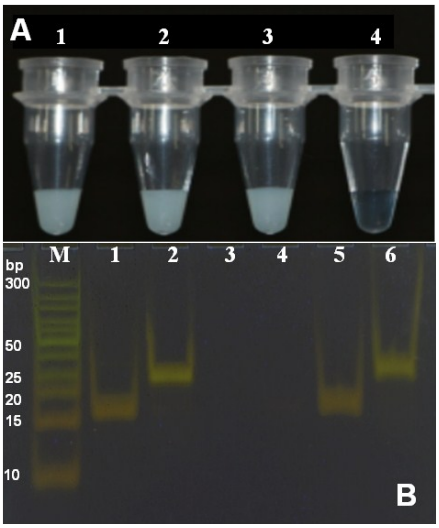

Fig. S4 (A) Photos of β-$Ni(OH)_2$ nanosheets (1) treated by adding 20 mM EDTA (2), heating at 95 °C (3) or both EDTA and heat (4). **(B)** Non-denatured PAGE analysis of the supernatant of different samples. Lane 1: 22-C; Lane 2: 22-C + DNA-141; Lane 3: 22-C + β-$Ni(OH)_2$ nanosheets +EDTA; Lane 4: 22-C + β-$Ni(OH)_2$ nanosheets + 95 °C heat treatment; Lane 5: 22-C + β-$Ni(OH)_2$ nanosheets +EDTA + 95 °C heat treatment; Lane 6: 22-C + β-$Ni(OH)_2$ nanosheets + EDTA + 95 °C heat treatment + DNA-141. Each sample contained a final buffer concentration of 25 mM, 100 mM KCl, 1 mM $MgCl_2$, 0.96 mg/mL β-$Ni(OH)_2$ nanosheets, 20 mM EDTA, and 2 μM DNA.

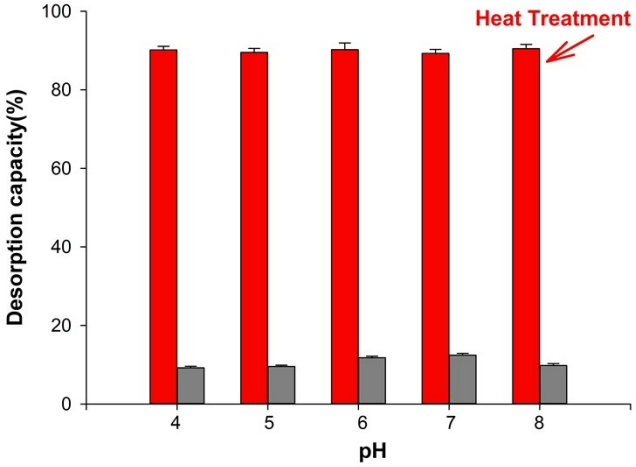

Fig. S5 Effect of pH on the desorption efficiency of DNA on β-$Ni(OH)_2$ nanosheets. Each sample (25 μL) contained a final buffer concentration of 25 mM, 100 mM KCl, 1 mM $MgCl_2$, 0.96 mg/mL β-$Ni(OH)_2$ nanosheets, 20 mM EDTA, and 2 μM DNA.

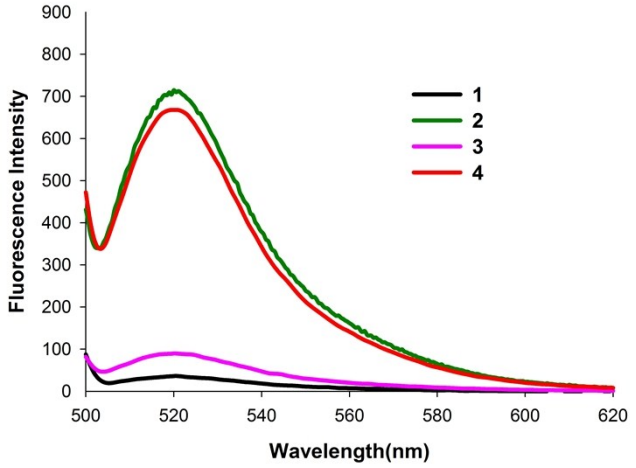

Fig. S6 Fluorescence response of MB for different samples. MB was used as a signal probe to recognize DNA-141. The fluorescence signal is low when there is no DNA-141 in the sample 1. The fluorescence signal is dramatically increased as the addition of DNA-141 in the sample 2 (1200 nM, 20 μL). We diluted sample 2 with buffer for 50-fold (sample 3: 24 nM, 20 μL), and then added β-$Ni(OH)_2$ nanomaterial to adsorb and enrich DNA-141 (sample 3': 24 nM, 1000 μL). After centrifugation and degradation, the adsorbed and enriched DNA-141 was desorbed and collected in sample 4 (20 μL). The sample 4 was also analyzed by MB. The signal induced by sample 4 with desorbed DNA-141 was approach with the sample before diluted sample 2.

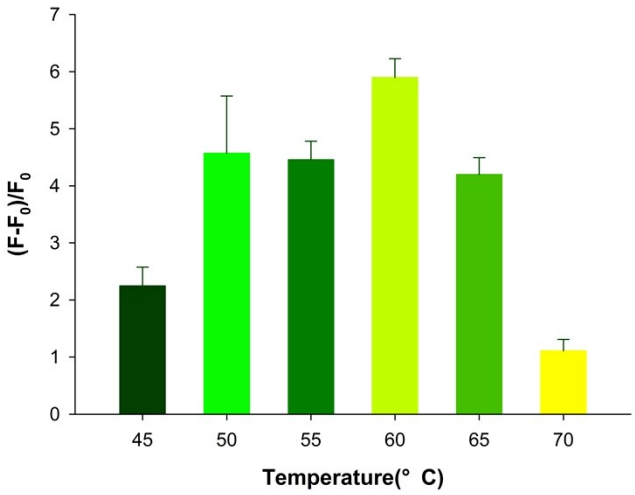

Fig. S7 The performance of the assay was evaluated by the $(F-F_0)/F_0$ at different temperatures, where F_0 and F are the fluorescence signals in the absence and the presence of miRNA-141, respectively. The concentrations of 22-F, miRNA and β-$Ni(OH)_2$ nanosheets were 300 nM, 10 nM ,10 nM and 6 μL (480 μg/mL), respectively. Error bars are standard deviation of three repetitive experiments.

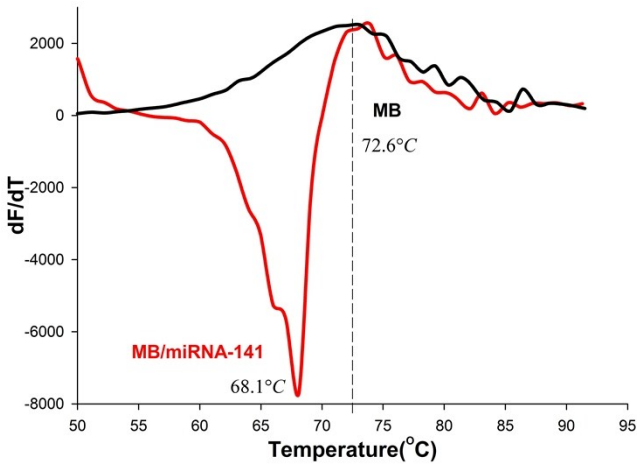

Fig. S8 Melting curve of MB/miRNA-141 duplex. The Tm of MB/miRNA-141 is about 68 ℃ which is higher than the working temperature of DSN (60℃). The underlined sequence of MB(5'-FAM-**CCTCCAC**CCATCTTTACCAGACAGTGTTA**GTGGAGG**-BHQ1-3') is designed to recognize miRNA-141 and form MB/miRNA-141 duplex. The experiment was performed on a Mx 3005P real-time PCR equipment (Stratagene, USA).

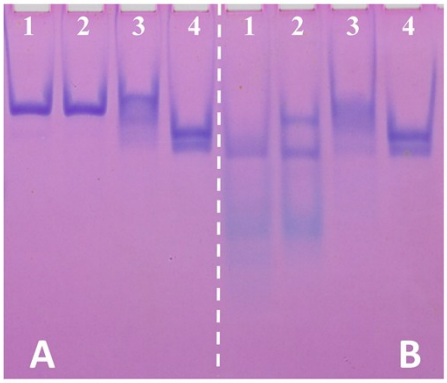

Fig. S9 Non-denatured PAGE analysis of P-141 and miRNAs in the absence **(A)** and presence **(B)** of DSN. Lane 1: P-141+ miRNA-141; Lane 2: P-141+ SmiRNA-141; Lane 3: P-141+ miRNA-429; Lane 4: P-141+ miRNA-21. The concentrations of P-141, miRNA and DSN were 2000 nM, 2000 nM and 0.4 U, respectively.

Table S2. Average Ct values in qRT-PCR assay of miRNA-141[a].

Cell Sample	miRNA-141	U6	ΔCt	ΔΔCt	$2^{(-\Delta\Delta Ct)}$
22Rv1	18.41899	8.033598	10.3854	0	1
293T	26.92119	7.931848	18.98934	8.603945	0.00257
MDA-MB231	18.07741	8.019919	10.05749	-0.32791	1.255191
HeLa	27.18598	7.833008	19.35297	8.967577	0.001998

[a] Detection of miRNA-141 expression levels in total RNA isolated from four kinds of human cell lines using qRT-PCR method. For each sample, we added the same dosage of total RNAs. U6 was used as reference gene. The values of $2^{-(\Delta\Delta Ct)}$ were relative with the expression levels. Relative expression levels were based on the expression ratio of miRNA-141 in target cell lines versus that in 22Rv1 cell lines. From the the values of $2^{-(\Delta\Delta Ct)}$, the expression level of miRNA-141 in 22Rv1 and MDA-MB231 cell line were estimated to be more than 400-fold of that in 293T and HeLa cell line, indicating the up-regulation of miRNA-141 in 22Rv1 and MDA-MB231cell lines as compared with 293T and HeLa cell lines.